Journal of Colloid and Interface Science 699 (2025) 138144

Contents lists available at ScienceDirect

Journal of Colloid And Interface Science

journal homepage: www.elsevier.com/locate/jcis

Regular Article

In situ generation of anti-leukemia vaccine by immunogenic dual-drug nanomedicine and polymersomal CpG nanoadjuvant

Lanlan Liang [a], Zhenzhen Zhai [a], Wenhai Lin [a], Li Cao [b], Huanli Sun [a,*], Zhiyuan Zhong [a,b,c,**]

[a] State Key Laboratory of Bioinspired Interfacial Materials Science, and Biomedical Polymers Laboratory, College of Chemistry, Chemical Engineering and Materials Science, Soochow University, Suzhou 215123, PR China
[b] College of Pharmaceutical Sciences, Soochow University, Suzhou 215123, PR China
[c] International College of Pharmaceutical Innovation, Soochow University, Suzhou 215222, PR China

HIGHLIGHTS

- NanoVi/Vo boosts robust ICD effects and antigen generation in AML cells.
- Combining nanoVi/Vo with nanoCpG adjuvants effectively stimulates DC maturation and cytokine release.
- The combination of nanoVi/Vo and nanoCpG elicits a potent *in situ* vaccination effect and enhances anti-AML immunotherapy.
- Combining nanoVi/Vo with nanoCpG substantially inhibits leukemia growth and improves survival benefit in AML-bearing mice.

GRAPHICAL ABSTRACT

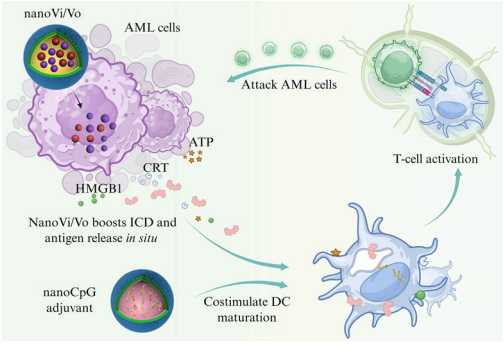

ARTICLE INFO

Keywords:
Acute myeloid leukemia
Polymersomes
Immunogenic cell death
Cancer vaccines
Immunoadjuvant

ABSTRACT

Acute myeloid leukemia (AML) is difficult to treat because of the difficulty in completely removing leukemia cells. Therapeutic vaccines that show promise in curing different cancers have achieved relatively little progress in the treatment of AML. Herein, we report the facile *in situ* generation of an anti-AML vaccine via an immunogenic vincristine/volasertib dual-drug nanomedicine (nanoVi/Vo) and a polymersomal CpG immunoadjuvant (nanoCpG). NanoVi/Vo boosted the generation of diverse tumor antigens by inducing immunogenic cell death (ICD) while synergistically inhibiting the growth of AML cells. Combining nanoVi/Vo with nanoCpG provoked a strong vaccination effect, which efficiently promoted dendritic cell (DC) maturation and facilitated T-cell activation and infiltration in the bone marrow, eliciting strong antitumor immunity in an orthotopic WEHI-3-Luc AML model. Notably, nanoVi/Vo combined with nanoCpG substantially suppressed leukemia progression in the bone marrow and infiltration to other organs, resulting in a significant survival benefit, with 57% of the mice surviving. This *in situ* vaccine generation strategy has promising potential as an effective immunotherapy approach for AML.

* Corresponding author.
** Corresponding author at: State Key Laboratory of Bioinspired Interfacial Materials Science, and Biomedical Polymers Laboratory, College of Chemistry, Chemical Engineering and Materials Science, Soochow University, Suzhou 215123, PR China.
E-mail addresses: sunhuanli@suda.edu.cn (H. Sun), zyzhong@suda.edu.cn (Z. Zhong).

https://doi.org/10.1016/j.jcis.2025.138144
Received 20 April 2025; Received in revised form 24 May 2025; Accepted 8 June 2025
Available online 9 June 2025

1. Introduction

AML is one of the most refractory hematological malignancies, with an inferior prognosis and a 5-year overall survival rate of less than 28 % [1,2]. Despite recent advances in molecular targeted drugs and their combination with standard chemotherapy, most patients are still intractable as a result of incomplete depletion of leukemia cells, which can cause relapse [3–7]. Therapeutic cancer vaccines are deemed to eradicate residual tumor cells and induce tumor regression by educating the host's immune system [8–11]. For example, personalized cancer vaccines that codeliver tumor-derived antigens and immunoadjuvants have demonstrated promising efficacy in treating different tumor models, including AML [12,13]. However, personalized cancer vaccines often result in suboptimal immune responses due to the weak immunogenicity of antigens and involve a tedious process [14,15].

In situ cancer vaccines, which employ endogenous tumor antigens at the tumor site to provoke effective antitumor immune responses, can overcome the abovementioned challenges and offer great potential for treating tumors [16,17]. The ICD is one of the key strategies used to generate *in situ* vaccines and can release tumor-associated antigens, thus stimulating DC maturation and T-cell activation and promoting antitumor immunity [18–21]. For example, most anthracycline and antimicrotubule chemotherapeutics have been demonstrated to induce ICD during the killing of tumor cells, which increases therapeutic efficacy via chemoimmunotherapy [22–24]. However, their low delivery efficiency, tendency toward drug resistance and potential for immune system impairment due to severe toxicity have significantly hampered their clinical efficacy. In recent years, chemotherapeutic-based ICD inducers have been loaded into nanoparticles to enhance tumor drug delivery, thus amplifying the ICD effects and reducing toxicity [25–27]. For example, Park et al. reported that loading doxorubicin into self-immolative polymeric micelles significantly enhanced its ICD effect and antitumor activity in a breast tumor mouse model [28]. However, the therapeutic efficacy of most single chemotherapeutic-loaded ICD nanoinducers remains suboptimal, likely because of uncontrollable drug release and drug resistance.

In this work, we report on potent *in situ* anti-AML vaccination via immunogenic dual-drug polymersomes containing vincristine sulfate and the polo-like kinase 1 (PLK1) inhibitor volasertib (nanoVi/Vo), in combination with nanoCpG (Scheme 1). PLK1 inhibitors, which specifically target PLK1, an oncogene closely associated with chemoresistance and poor prognosis, can sensitize lung cancer cells to chemotherapy and have recently been shown to induce ICD [29,30]. CpG, a well-known Toll-like receptor 9 (TLR9) agonist that can activate DCs and potentiate the innate immune system, is a widely explored vaccine adjuvant to increase the immunogenicity of cancer vaccines [31–33]. Our recent work demonstrated that, compared with free CpG, nanoCpG substantially enhances immune responses in solid tumors and enables systemic injection by overcoming the limitations of CpG itself, such as its susceptibility to degradation and lower cellular uptake [34]. NanoVi/Vo

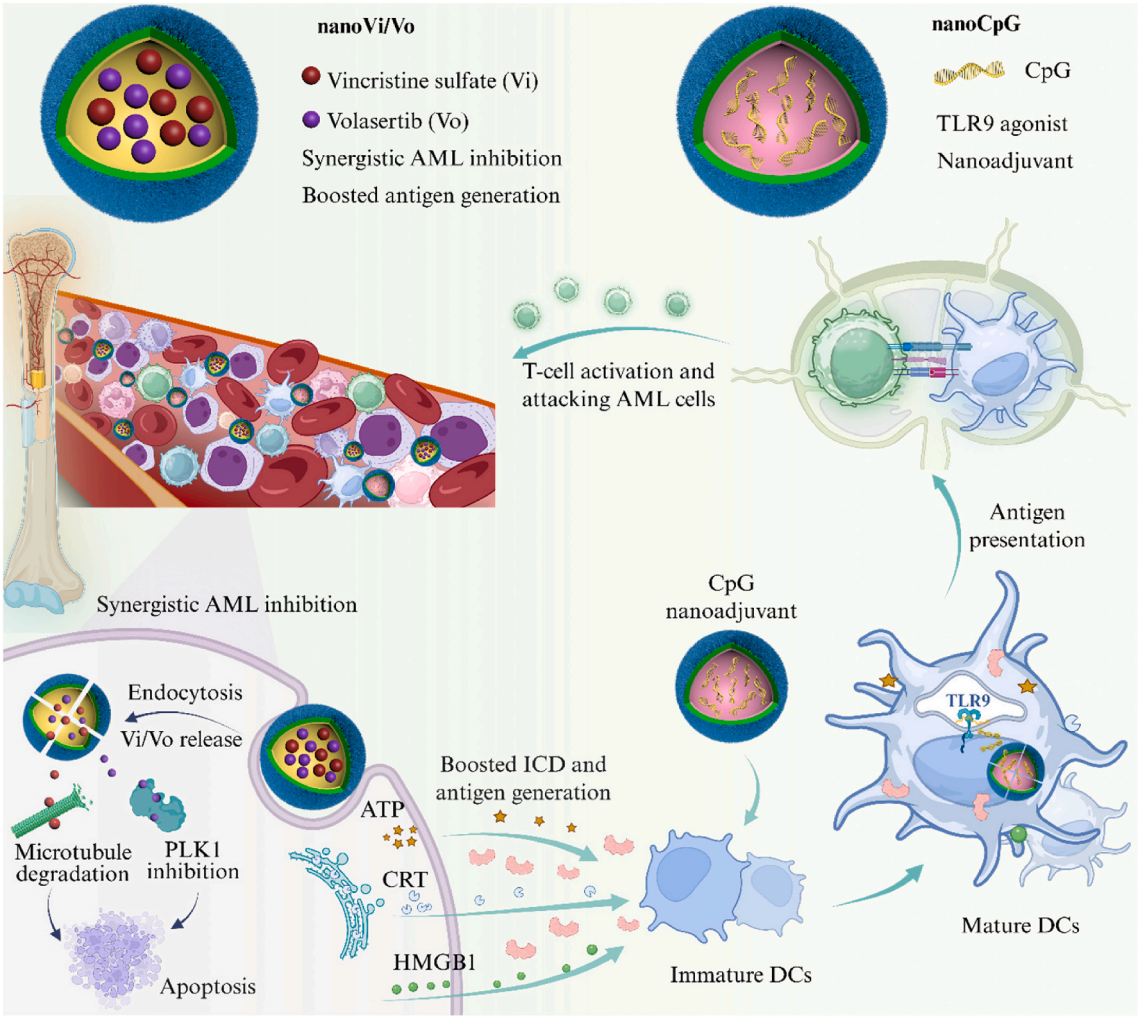

Scheme 1. Schematic showing that nanoVi/Vo enhances ICD and the generation of tumor antigens while synergistically inducing apoptosis in AML cells, which, in combination with the nanoCpG adjuvant, elicits robust *in situ* vaccines to enhance anti-AML immunotherapy.

synergistically increased ICD and the generation of diverse tumor antigens, which, in combination with nanoCpG, promoted DC maturation, T-cell activation and immune cell infiltration at the leukemic site. Notably, combining nanoVi/Vo with nanoCpG significantly inhibited leukemia progression and invasion to major organs in an orthotopic WEHI-3-Luc AML mouse model, with 57 % of the mice surviving for at least 75 days.

2. Materials and methods

2.1. Materials

CpG ODN 1826 (> 95 %, Sangon Biotech (Shanghai) Co., Ltd.), vincristine sulfate (Vi, 99.9 %, Dalian Meilun Biotechnology Co., Ltd.), volasertib (Vo, 99.4 %, Med Chem Express), D-luciferin potassium salt (99 %, Bridgen Co., Ltd.), 3-(4,5-dimethylthiazol-2-yl)-2,5-diphenyltetrazolium bromide (MTT, 99.9 %, Macklin Biochemical Co., Ltd.), 4 % paraformaldehyde tissue fixative (Biosharp Life Sciences), and cell counting kit-8 (CCK-8, Shanghai Enzyme-linked Biotechnology Co., Ltd.) were used as received. N,N-Dimethylformamide (DMF, > 99.5 %) and dimethyl sulfoxide (DMSO, > 99.5 %) were obtained from Sinopharm Chemical Reagent Co., Ltd. Poly(ethylene glycol)-*b*-poly(trimethylene carbonate-*co*-dithiolane trimethylene carbonate)-*b*-*N*-terminally acetylated poly(aspartic acid) (PEG-P(TMC-DTC)-Ac-KD_{10}, M_n: 5.0-(15.1–2.0)-1.3 kg/mol) and PEG-P(TMC-DTC)-SP (M_n: 5.0-(14.5–2.0)-0.2 kg/mol, SP: spermine) were synthesized as described in our previous reports [35,36].

Apoptosis kit (MultiSciences Biotech Co., Ltd.), enhanced adenosine triphosphate (ATP) assay kit (Beyotime Biotechnology, S0027), high mobility group box chromosomal protein 1 (HMGB1) enzyme-linked immunosorbent assay (ELISA) kit (MB-5840A, Meibiao Biotechnology), ELISA kits for mouse interferon-γ (IFN-γ), interleukin-6 (IL-6), interleukin-12 p70 (IL-12p70), and tumor necrosis factor-α (TNF-α) (InvivoGen), eBioscience™ FoxP3/Transcription Factor Staining Buffer Set (Invitrogen, 2400631), calreticulin (CRT) antibody (Abcam, Ab2907), Alexa Fluor 647-conjugated goat anti-rabbit IgG H&L (Invitrogen), and anti-mouse CD16/CD32 antibody (Selleck) were used according to the manufacturers' protocols. Zombie NIR™ and fluorescently labeled antibodies for mouse markers, including CD45-PerCP/Cyanine5.5, CD45-PE, CD3-FITC, CD8-PE, CD8-PE/Cy7, CD4-PE, IFN-γ-APC, TNF-α-PerCP/Cyanine5.5, Granzyme B-PE, Perforin-APC, CD107a-Alexa Fluor 647, CD25-PE/Cy7, FoxP3-Alexa Fluor 647, CD11c-FITC, CD80-APC, CD86-PE/Cy7, CD86-PE, MHC II-PerCP/Cyanine5.5, CD11b-FITC, F4/80-PE, and CD206-Alexa Fluor 647, were purchased from BioLegend and used as instructed.

2.2. Cell source and culture

Murine WEHI-3 AML cells tagged with luciferase (WEHI-3-Luc) were provided by the Institute of Hematopoietic Stem Cell Transplantation, Soochow University. Human T cells isolated from the peripheral blood of healthy donors were obtained from the Hematology Research Center of the Tang Zhongying Medical Institute, Soochow University. WEHI-3-Luc cells were cultured in RPMI-1640 medium (HyClone) supplemented with 10 % fetal bovine serum (Gibco) and 1 % penicillin–streptomycin at 37 °C under 5 % CO_2. Bone marrow-derived dendritic cells (BMDCs) were isolated from the femurs of healthy female BALB/c mice (6 weeks old, 18–20 g, Vital River Laboratory Animal Technology Co., Ltd., Beijing). Briefly, the mice were euthanized and sterilized with ethanol, and the femurs were aseptically excised. Bone marrow cells were flushed with RPMI-1640 medium, filtered through a cell strainer, and treated with ammonium chloride potassium (ACK) lysis buffer to remove erythrocytes. The cells were then seeded at 5×10^5 mL in complete RPMI-1640 medium supplemented with 20 ng/mL granulocyte–macrophage colony-stimulating factor (designated day 0). The medium was replenished with fresh medium on day 3, and the BMDCs were harvested on day 6.

2.3. Characterizations

The hydrodynamic diameter and size distribution of the polymersomes were measured via a ZetaSizer Nano-ZS dynamic light scattering (DLS) instrument equipped with a 633 nm He-Ne laser. The concentrations of Vi and Vo were determined via high-performance liquid chromatography (HPLC, Waters 2695) with a C18 reverse-phase column (Sepax BR-C18, 5 μm, 4.6 × 250 mm). The mobile phase consisted of acetonitrile/water (60/40, v/v) at a flow rate of 1 mL/min, with UV detection wavelengths of 298 nm and 330 nm, respectively. The concentration of CpG was quantified via a NanoDrop 2000 spectrophotometer (Thermo Scientific). The levels of HMGB1 and cytokines (IFN-γ, IL-6, IL-12p70, and TNF-α) were assessed via ELISA, with detection performed on a Thermo Varioskan LUX multimode microplate reader. Hematoxylin and eosin (H&E) staining images were captured via an inverted fluorescence microscope (Nikon Eclipse Ti). Apoptosis, CRT surface expression, BMDC maturation, and immune cell populations were analyzed via flow cytometry (BD FACS). Bioluminescent signals in the mice were detected via an IVIS Lumina II imaging system, and the data were processed with Living Image 2.6 software.

2.4. Preparation of nanoVi/Vo and nanoCpG

NanoVi/Vo was fabricated through one-step self-assembly of a PEG-P(TMC-DTC)-Ac-KD_{10} amphiphilic copolymer with simultaneous loading of Vi and Vo. The Vi/Vo feeding mass ratio was set at 1:16 on the basis of our previous study to obtain nanoVi/Vo with an actual Vi/Vo mass ratio of 1:24, which has been demonstrated to have the strongest synergistic effect in acute lymphoblastic leukemia cells [37]. In brief, a Vi solution (5 mg/mL) was mixed with N-2-hydroxyethylpiperazine-N-2-ethane sulfonic acid buffer (HEPES, 5 mM, pH 6.8) under stirring, followed by slow injection with a mixture of PEG-P(TMC-DTC)-Ac-KD_{10} (DMSO, 40 mg/mL) and Vo solutions (DMSO, 20 mg/mL). After stirring for 30 min and incubation for 24 h, the suspension was dialyzed (MWCO: 3.5 kDa) against HEPES (5 mM, pH 7.4) for 6 h to obtain nanoVi/Vo. Similarly, nanoCpG was prepared by injecting a DMF solution of PEG-P(TMC-DTC)-SP into phosphate buffer (PB, 2 mM, pH 6.0) containing CpG, and the theoretical drug loading content (DLC) of CpG was 5 wt%. The size and polydispersity index (PDI) of nanoVi/Vo and nanoCpG were measured via DLS. The amounts of Vi and Vo in nanoVi/Vo were determined via HPLC, and the content of CpG was determined via a NanoDrop on the basis of the corresponding standard curves. The DLC and drug loading efficiency (DLE) were then calculated via the following formulas.

$$\mathrm{DLC\,(wt.\%)} = \frac{\text{weight of loaded drug}}{\text{weight of drug loaded polymersomes}} \times 100$$

$$\mathrm{DLE\,(\%)} = \frac{\text{weight of loaded Vi, Vo or CpG}}{\text{weight of Vi, Vo or CpG in feed}} \times 100$$

2.5. In vitro anti-AML effects of nanoVi/Vo

The anti-AML effect of nanoVi/Vo was evaluated in murine WEHI-3-Luc cells, with nanoVi and nanoVo single-drug polymersomes as well as a physical mixture of nanoVi and nanoVo (nanoVi + nanoVo) used as controls. The cells were plated in 96-well plates at a density of 3×10^3 cells per well and incubated with various concentrations of nanoVi, nanoVo, nanoVi/Vo and nanoVi + nanoVo for 48 h (n = 6). Subsequently, 10 μL of MTT solution (5 mg/mL) was added to each well for another 4 h of incubation. The medium of each well was then aspirated and replaced with 150 μL of DMSO to dissolve the formazan, and its absorbance at 570 nm was determined via a microplate reader. Cell viability was calculated, and dose–response curves were fitted via

GraphPad Prism to obtain the half-maximal inhibitory concentration (IC_{50}) values. The combination index (CI) for Vi and Vo was calculated via the following formula:

$$CI = \frac{IC_{50} \text{ of Vi in combination}}{IC_{50} \text{ of nanoVi}} + \frac{IC_{50} \text{ of Vo in combination}}{IC_{50} \text{ of nanoVo}}$$

The CI value signifies synergistic (<1), additive (=1), or antagonistic (>1) effects.

Normal human T cells and mouse BMDCs were used as controls to evaluate the toxicity of nanoVi/Vo via a CCK-8 kit. The cells plated in 96-well plates (2×10^4 cells per well) were incubated with nanoVi, nanoVo, or nanoVi/Vo at various concentrations. After 48 h of incubation in the incubator, 10 μL of CCK-8 solution was added to each well for an additional 4 h of incubation. The absorbance of each well at 450 nm was measured via a microplate reader, and the cell viability was calculated (n = 6).

An Annexin V-PE/7-AAD apoptosis kit was used to assess the synergistic proapoptotic effect of nanoVi/Vo in AML cells (n = 3). WEHI-3-Luc cells plated in 12-well plates (3×10^5 cells per well) were incubated with phosphate-buffered saline (PBS), nanoVi, nanoVo or nanoVi/Vo for 24 h at different Vi (1, 2, or 5 ng/mL) and/or Vo concentrations (24, 48, or 120 ng/mL). Afterwards, the cells were collected via centrifugation and resuspended in 0.5 mL of binding buffer. Then, 5 μL of Annexin V-PE and 10 μL of 7-AAD solution were added, and the cells were stained at room temperature for 5 min. The cells were subsequently analyzed via flow cytometry. The data were analyzed via FlowJo_V10 software.

2.6. NanoVi/Vo-induced ICD effects

The ICD effect of nanoVi/Vo was evaluated in WEHI-3-Luc cells by determining typical ICD markers, including CRT, ATP and HMGB1 (n = 3). The cells were plated in 12-well plates (2×10^5 cells per well) and incubated with nanoVi (Vi: 1, 5 ng/mL), nanoVo (Vo: 24, 120 ng/mL), or nanoVi/Vo (Vi/Vo: 1/24 ng/mL) for 24 h. Afterwards, the culture medium was collected to measure the ATP and HMGB1 levels via an enhanced ATP assay kit and an HMGB1 ELISA kit, respectively. The cells were collected and sequentially stained with the CRT antibody and Alexa Fluor 647-labeled goat anti-rabbit IgG H&L on ice for 1 h and 30 min, respectively. After each staining step, the cells were washed twice with PBS. CRT expression on the surface of WEHI-3-Luc cells was subsequently analyzed via flow cytometry.

2.7. BMDC maturation stimulated by the nanoVi/Vo-induced ICD effect and nanoCpG

WEHI-3-Luc cells were seeded in 12-well plates (1×10^5 cells/well) and treated with nanoVi, nanoVo, nanoVi/Vo, or PBS for 24 h at Vi and/or Vo concentrations of 1 and 24 ng/mL. After incubation, BMDCs (1×10^6 cells/mL/well) were added to each well. Subsequently, nanoCpG (1 μg/mL) was added to three PBS- or nanoVi/Vo-treated wells. All the groups were further incubated for 24 h. The cells were then collected by centrifugation and blocked with 25 μL of anti-CD16/32 antibody at 4 °C for 10 min, followed by the addition of a mixed solution (50 μL) of CD11c-FITC (diluted 1:200), CD80-APC and CD86-PE antibodies (diluted 1:400). The cells were then incubated on ice in the dark for 30 min and washed twice with PBS. Finally, flow cytometry was used to detect $CD11c^+CD80^+CD86^+$ mature BMDCs. Moreover, the culture medium was collected to determine the levels of the cytokines TNF-α, IL-6, and IL-12p70 by corresponding ELISA kits.

Similarly, BMDCs were directly incubated for 24 h with PBS, nanoVi, nanoVo, nanoVi/Vo, nanoCpG, or a combination of nanoVi/Vo + nanoCpG at Vi, Vo, and CpG concentrations of 1 ng/mL, 24 ng/mL, and 1 μg/mL, respectively, and analyzed by flow cytometry after staining.

2.8. In vivo anti-AML efficacy of nanoVi/Vo in combination with nanoCpG

All the animal experiments were approved by the Animal Care and Use Committee of Soochow University, and all the protocols conformed to the Guide for the Care and Use of Laboratory Animals (Approval No: SYXK 2021–0065). The *in vivo* anti-AML activity of nanoVi/Vo in combination with nanoCpG was evaluated in an orthotopic murine WEHI-3-Luc AML model, which was established via tail vein injection of 6×10^6 WEHI-3-Luc cells into each BALB/c mouse (6 weeks old, Charles River). The day of tumor inoculation was designated day 0. Leukemia progression was monitored via the detection of bioluminescence signals derived from WEHI-3-Luc cells. D-luciferin potassium salt was used as a substrate for luciferase, and it was intraperitoneally injected into each mouse at a dose of 75 mg/kg 10 min prior to *in vivo* bioluminescence imaging. When the average bioluminescence signal reached approximately 10^7 photons per second (p/s), the mice were randomly divided and intravenously injected with nanoVi/Vo at three different doses (Vi/Vo: 0.028/0.67, 0.083/2, and 0.25/6 mg/kg) along with nanoCpG (CpG: 1 mg/kg) to optimize the dosing regimen. Mice treated with PBS served as controls. NanoVi/Vo was injected via the tail vein every 3 days for a total of 4 injections, and nanoCpG was injected via the tail vein approximately 15 h after each nanoVi/Vo injection. Twenty-four hours after the last injection of nanoCpG, the mice were euthanized, and their peripheral blood, bone marrow, spleen, and lymph nodes were collected for immune analysis. The blood samples were lysed with ACK lysis buffer, and the other samples were processed into single-cell suspensions through grinding, filtering, and centrifugation. Subsequently, 100 μL of Zombie NIR solution (1:200 dilution) was added to each sample and incubated at room temperature in the dark for 15 min for dead cell staining. After being washed with PBS, the cells were blocked with an anti-CD16/32 antibody on ice for 10 min. Antibodies specific for cytokine-secreting T cells (CD3-FITC, CD4-PE, CD8-PE/Cy7, IFN-γ-APC, TNF-α-PerCP/Cyanine5.5), CD107a-positive T cells (CD3-FITC, CD4-PE, CD8-PE/Cy7, CD107a-Alexa Fluor 647), Tregs (CD3-FITC, CD4-PE, CD25-PE/Cy7, FoxP3-Alexa Fluor 647), and DCs (CD45-PE, CD11c-FITC, MHC-II-PerCP/Cyanine5.5, and CD86-PE/Cy7) were subsequently added and incubated on ice in the dark for 30 min. FITC-labeled antibodies were diluted 200 times, and the other antibodies were diluted 400 times. Finally, the cells were washed with PBS and resuspended in 1 % paraformaldehyde solution. Flow cytometry was used to detect the proportions of T cells, Tregs, and DCs.

The anti-AML activity of nanoVi/Vo at the optimal dosage (Vi/Vo: 0.25/6 mg/kg) in combination with nanoCpG was subsequently assessed. On day 10, when the average bioluminescence signal reached 10^7p/s, the mice were divided into four groups and treated with PBS, nanoVi/Vo, nanoCpG, or nanoVi/Vo + nanoCpG. NanoVi/Vo was administered on days 10, 13, 16, and 19, and the combination group received nanoCpG 15 h after each nanoVi/Vo injection. The group receiving nanoCpG alone was injected at the same time points as the combination group. Each group consisted of 14 mice: 7 for monitoring body weight, survival, and tumor growth; 4 for detecting immune cells and cytokine secretion *in vivo*; and 3 for blood routine and leukemia infiltration analysis. Leukemia progression in the mice was monitored through bioluminescence imaging every 7 days.

To analyze immune cells, mouse serum was collected 6–8 h after the last injection of nanoCpG, and the concentrations of proinflammatory cytokines (IFN-γ, TNF-α, and IL-12p70) were measured via ELISA kits. Twenty-four hours after the last injection of nanoCpG (21 days post leukemia inoculation), 4 mice from each group were euthanized, and the bone marrow, spleen, and lymph nodes were collected to prepare single-cell suspensions, following the same procedures as those described above. Finally, antibody staining was performed, and the proportions of T cells, Tregs, DCs, and macrophages in various organs were detected via flow cytometry. The following cellular markers were used: cytokine-secreting T cells (CD3-FITC, CD4-PE, CD8-PE/Cy7, IFN-γ-APC, TNF-

α-PerCP/Cyanine5.5), T cells secreting granzyme B or perforin (CD45-PerCP/Cyanine5.5, CD3-FITC, CD8-PE/Cy7, Granzyme B-PE, Perforin-APC), CD107a-positive T cells (CD45-PerCP/Cyanine5.5, CD3-FITC, CD8-PE, CD107a-Alexa Fluor 647), Tregs (CD45-PerCP/Cyanine5.5, CD3-FITC, CD4-PE, FoxP3-Alexa Fluor 647), DCs (CD45-PE, CD11c-FITC, MHC-II-PerCP/Cyanine5.5, CD86-PE/Cy7, CD80-APC), and macrophages (CD45-PerCP/Cyanine5.5, CD11b-FITC, F4/80-PE, CD86-PE/Cy7, CD206-Alexa Fluor 647).

On day 21 post leukemia inoculation, 3 mice from each group designated for blood routine and leukemia cell infiltration analysis were euthanized. Peripheral blood was collected for routine blood testing, and major organs and limbs were collected for ex vivo bioluminescence

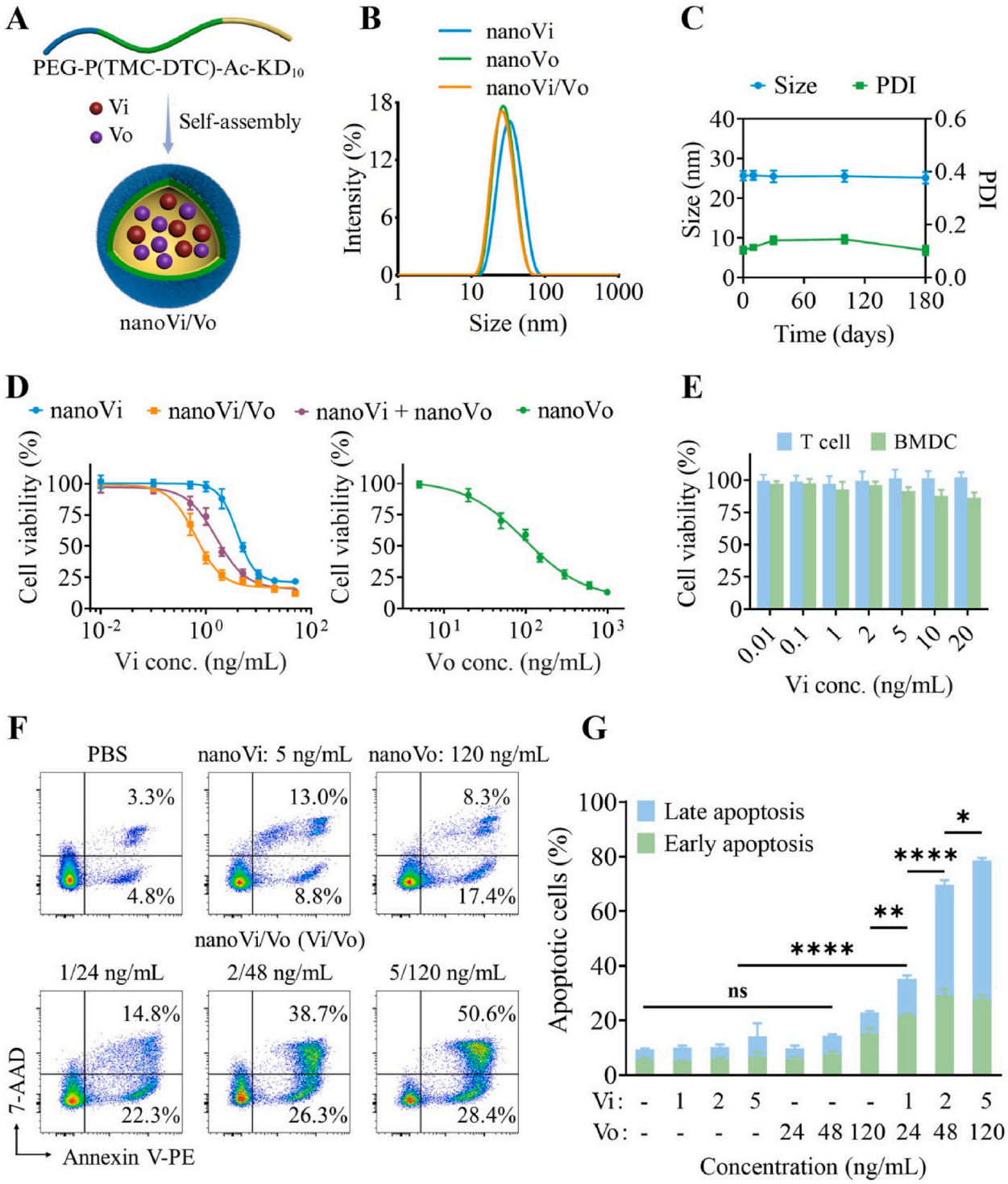

Fig. 1. (A) Schematic diagram of the preparation of nanoVi/Vo. (B) Size distributions of nanoVi, nanoVo, and nanoVi/Vo. (C) Changes in the particle size and PDI of nanoVi/Vo during storage at 4 °C for 180 days (n = 3). (D) Viability of WEHI-3-Luc cells after incubation with nanoVi/Vo, nanoVi, nanoVo, or nanoVi + nanoVo mixture for 48 h (n = 6). (E) Viability of normal human T cells and mouse BMDCs after incubation with nanoVi/Vo for 48 h (n = 6). (F) Representative flow cytometry patterns and (G) quantitative analysis showing the apoptosis of WEHI-3-Luc cells after incubation with different formulations (n = 3). *p < 0.05, **p < 0.01, ****p < 0.0001.

imaging and histological analysis. Healthy BALB/c mice were used as controls. Additionally, the hindlimbs of one mouse from each group were embedded, sectioned, and subjected to immunofluorescence analysis for *in vivo* ICD markers (CRT^+), as well as immunofluorescence imaging analysis of cytotoxic T cells ($CD8^+$ T, CTL) and $CD11c^+CD86^+$ DC cells.

2.9. Statistical analysis

The data are presented as the means ± standard deviations (SDs) and were analyzed via GraphPad Prism 8.0. Statistical comparisons between groups were conducted via one-way ANOVA. For survival curves, statistical significance was assessed via the log-rank (Mantel–Cox) test. *p < 0.05, **p < 0.01, ***p < 0.001, and ****p < 0.0001.

3. Results and discussion

3.1. Preparation and in vitro anti-AML activity of nanoVi/Vo

This study aims to program *in situ* vaccines via the synergistic induction of ICD and the activation of pattern recognition receptors (PRRs), thus restoring the cancer immune cycle. To stimulate the ICD effect, nanoVi/Vo was engineered to codeliver Vi and Vo ratiometrically to leukemia cells, thus increasing synergistic effects and reducing toxicity. The dissimilar properties of different drugs may cause different pharmacokinetics and biodistributions *in vivo*, leading to uncontrollable drug ratios in cancer cells and gloomy synergistic effects [38]. Nanoparticle-mediated ratiometric codelivery of different drugs is critical to translate the synergistic effects *in vitro* to *in vivo* [39]. The amphiphilic PEG-P(TMC-DTC)-Ac-KD_{10} triblock copolymer has been shown to assemble into chimeric polymersomes, with simultaneous disulfide crosslinking achieved via the ring-opening polymerization of dithiolane rings within the hydrophobic membrane. The negatively charged KD_{10} inner surface in chimeric polymersomes enables the effective encapsulation of proteins and positively charged small-molecule drugs through electrostatic interactions [40–42]. Herein, PEG-P(TMC-DTC)-Ac-KD_{10} based chimeric polymersomes were employed to coload Vi and Vo via electrostatic interactions to obtain nanoVi/Vo. Single-drug polymersomes (nanoVi and nanoVo) were prepared similarly and used as controls. NanoVi/Vo had a small size of 26 nm and a narrow size distribution (PDI: 0.11), which was close to that of nanoVi (31 nm, PDI: 0.09) and nanoVo (26 nm, PDI: 0.13) (Fig. 1**B and Table S1**). The DLEs of Vi and Vo in nanoVi/Vo were 47.8 % and 76.7 %, respectively, resulting in a Vi/Vo mass ratio of approximately 1:24 and a molar ratio of approximately 1:35. Notably, the resulting nanoVi/Vo was highly stable after 180 days of storage at 4 °C, with negligible changes in both size and PDI (Fig. 1**C**).

The anti-AML activity of nanoVi/Vo was assessed via the MTT assay in murine WEHI-3-Luc AML cells, with the nanoVi, nanoVo and a nanoVi + nanoVo mixture used as controls. NanoVi/Vo exhibited superior anti-AML activity to that of the single-drug polymersomes, with IC_{50} values of 0.8 and 19.0 ng/mL for Vi and Vo, which were 5.3- and 6.7-fold lower than those of nanoVi and nanoVo, respectively, resulting in a strong synergistic effect (CI: 0.3) (Fig. 1**D and Table S2**). However, the nanoVi + nanoVo physical mixture displayed 2.4-fold lower anti-AML activity and much weaker synergy (CI: 0.8) than did nanoVi/Vo, indicating the advantage of coloading Vi and Vo together. In addition, nanoVi/Vo showed no significant toxicity to normal human T cells or mouse BMDCs even at Vi/Vo concentrations up to 20/480 ng/mL (Fig. 1**E**), similar to nanoVi and nanoVo (**Fig. S1**).

Vi reportedly inhibits tubulin polymerization, disrupts the mitotic process, and arrests cells in the G2/M phase, thus leading to apoptosis [43]. Vo can also cause G2/M cell cycle arrest and apoptosis by inhibiting the activity of the PLK1 protein [44]. We therefore further studied the synergy of nanoVi/Vo in causing cell apoptosis via Annexin V-PE/7-AAD double staining. As shown in Fig. 1F, G, nanoVi/Vo induced dose-dependent cell apoptosis in WEHI-3-Luc cells, and the total apoptosis rate increased from 37.1 % to 65.0 % and 79.0 % when the Vi/Vo concentration increased from 1/24 to 2/48 and 5/120 ng/mL, respectively. Notably, the proapoptotic ability of nanoVi/Vo at Vi/Vo concentrations of 1/24 ng/mL not only contrasted sharply with that of nanoVi and nanoVo at equal drug concentrations, where no obvious cell apoptosis was observed, but also significantly surpassed that of nanoVi (21.8 %) and nanoVo (25.7 %) at a 5-fold higher concentration (Fig. S2)

3.2. NanoVi/Vo-induced ICD effects

Vo has been previously shown to induce ICD effect in cancer cells [45]. To assess the ability of Vi to potentiate the ICD effect of Vo in AML cells, WEHI-3-Luc cells incubated with nanoVi/Vo, nanoVi or nanoVo were subjected to flow cytometry analysis via the determination of typical ICD markers (CRT, HMGB1 and ATP). As shown in Fig. 2**A, B**, nanoVi/Vo treatment at Vi and Vo concentrations of 1 and 24 ng/mL significantly increased the proportion of CRT-positive cells from 4.7 % in the PBS group to 38.9 %. This increase was notably greater than that in cells treated with nanoVi (7.7 %) or nanoVo (9.6 %) at the same drug concentration or even at a 5-fold higher concentration (12.1 %, 14.9 %). Additionally, compared with other treatments, nanoVi/Vo markedly increased the secretion of ATP and HMGB1 by WEHI-3-Luc cells to the greatest extent (Fig. 2**C, D**).

The CRT, HMGB1 and ATP released during ICD are known to stimulate the maturation of antigen-presenting cells, particularly DCs, thus provoking tumor-specific immune responses. We therefore investigated the effects of nanoVi/Vo-induced ICD on DC maturation by coculturing mouse BMDCs with nanoVi/Vo-pretreated WEHI-3-Luc cells (Fig. 2**E**). The results revealed that the number of mature BMDCs (mDCs, $CD80^+CD86^+$) in the nanoVi and nanoVo groups increased by only 0.6–0.8 % compared with that in the PBS group (Fig. 2**F, G**), likely due to the limited ICD effect. In contrast, nanoVi/Vo-treated WEHI-3-Luc cells more efficiently promoted the maturation of BMDCs, with the percentage of mDCs increasing from 10.7 % (PBS group) to 18.5 %. However, nanoVi/Vo itself failed to stimulate BMDC maturation when incubated directly with BMDCs (**Fig. S3**), suggesting that the tumoral ICD effect plays a major role in stimulating DC maturation.

To increase the generation of *in situ* vaccines, cancer adjuvants such as CpG were further used to enhance anti-AML immunity. CpG can enhance antigen presentation in DCs by activating PRRs and has been utilized in clinical trials for cancer immunotherapy [33]. However, the use of CpG is limited by inefficient cellular uptake, rapid degradation and possible immunogenic toxicity *in vivo*. In this study, CpG was efficiently encapsulated into the polymersomes via self-assembly of the PEG-P(TMC-DTC)-SP copolymer according to our previous report [46]. The resulting nanoCpG had a size of 58 nm, a narrow size distribution (PDI: 0.09), a high DLE of 94.8 % and a uniform spherical structure (**Fig. S4A and Table S3**). NanoCpG also exhibited high stability against long-term storage, with minimal size changes and drug leakage over 180 days (**Fig. S4B, C**). Culturing BMDCs with nanoCpG for 24 h increased the percentage of mDCs to 19.5 %, which, in combination with the ICD induced by nanoVi/Vo, further promoted BMDC maturation to 32.1 % (Fig. 2**F, G**). Consistently, nanoVi/Vo-treated WEHI-3-Luc cells or nanoCpG effectively promoted the secretion of proinflammatory cytokines (IL-12p70, TNF-α and IL-6) by BMDCs, and the combination of both further significantly increased the levels of IL-12p70, TNF-α, and IL-6 (Fig. 2**H-J**). Taken together, these findings indicate that nanoVi/Vo can induce ICD in AML cells and generate diverse antigens that cooperate with nanoCpG to synergistically promote DC maturation.

3.3. Combining nanoVi/Vo with nanoCpG induces potent immunotherapeutic efficacy in a syngeneic AML model

Encouraged by the promising *in vitro* anti-AML and DC stimulation results, an orthotopic WEHI-3-Luc AML model was established to

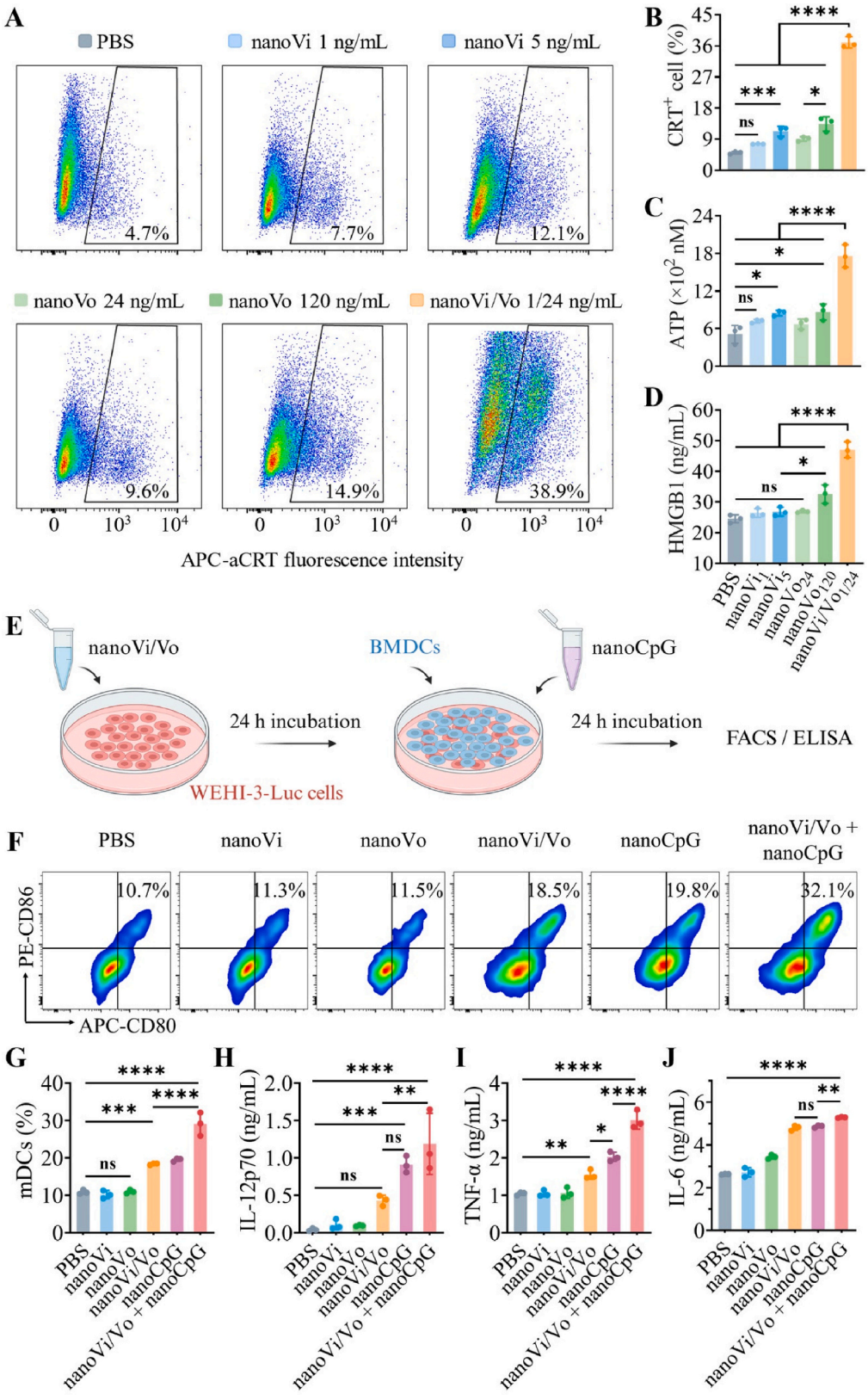

Fig. 2. The effect of nanoVi/Vo on ICD in WEHI-3-Luc cells and the subsequent stimulation of DC maturation. (A) Representative flow cytometry plots and (B) quantification of CRT-positive WEHI-3-Luc cells after incubation with nanoVi/Vo, nanoVi or nanoVo (n = 3). Concentrations of (C) ATP and (D) HMGB1 in the culture medium of WEHI-3-Luc cells treated with different formulations (n = 3). The numbers in the subscript denote the concentrations of Vi or Vo. (E) Experimental scheme for stimulating BMDC maturation with nanoVi/Vo-pretreated WEHI-3-Luc cells and nanoCpG. (F) Representative flow cytometry plots and (G) quantification of BMDC maturation promoted by different treatments (n = 3). Concentrations of secreted (H) IL-12p70, (I) TNF-α, and (J) IL-6 by BMDCs (n = 3). *p < 0.05, **p < 0.01, ***p < 0.001, ****p < 0.0001.

evaluate the immunotherapeutic effects of the combination of nanoVi/Vo and nanoCpG against AML (Fig. 3**A**). First, we explored the effects of nanoVi/Vo at three different dosages in combination with nanoCpG on the activation of the immune system. The results revealed that the activation of the immune response was dose dependent, with the most pronounced effect observed at Vi/Vo doses of 0.25/6 mg/kg (**Fig. S5**). Specifically, the percentages of $CD4^+$ and $CD8^+$ T cells that secrete IFN-γ and TNF-α, CD107a-positive $CD8^+$ T cells and $CD86^+$/MHC-II^+ DCs were notably increased. Subsequently, anti-AML studies of nanoVi/Vo + nanoCpG were performed at Vi, Vo and CpG dosages of 0.25, 6 and 1 mg/kg, respectively. NanoVi/Vo, nanoCpG or PBS served as controls. The treatment was initiated on day 10 after inoculation, when the average bioluminescence signal of the mice reached approximately 10^7p/s. In PBS-treated mice, bioluminescence signals from leukemia cells were first detected in the hindlimbs and then exponentially increased and rapidly spread throughout the body over time (Fig. 3**B, C**), leading to weight loss, hindlimb paralysis, and death. Notably, treatment with nanoVi/Vo + nanoCpG significantly inhibited the proliferation of leukemia cells, with 5 out of 7 mice showing undetectable bioluminescence signals on day 38 following implantation. However, treatment with either nanoVi/Vo or nanoCpG alone only partially inhibited the proliferation of leukemia cells during the first week, which was subsequently renewed and exhibited a dramatic growth trend similar to that observed in PBS-treated mice. Accordingly, the nanoVi/Vo + nanoCpG combination treatment significantly extended the survival of the mice, with 4 out of the 7 mice surviving for at least 75 days, which was significantly superior to that of the PBS group (25 days), nanoVi/Vo (38 days) or nanoCpG (33 days) treatment alone (Fig. 3**D**). Moreover, no significant weight loss was observed in the mice treated with nanoVi/Vo or nanoCpG alone or with their combination (Fig. 3**E**).

Leukemic infiltration in the bone marrow and extramedullary organs is one of the typical features of AML patients [47,48]. *Ex vivo* bioluminescence imaging revealed that PBS-treated mice suffered severe leukemia burdens in the liver, spleen, lungs, and hindlimbs, whereas nanoVi/Vo + nanoCpG treatment efficiently inhibited leukemia infiltration in different tissues, with no detectable bioluminescence signals (Fig. 3**F and S6**). H&E-stained images provided further evidence that mice in the combination treatment group presented normal histological morphology in major organs and bone marrow, similar to that of healthy mice (**Fig. S7, S8**). The abnormal proliferation and accumulation of leukemia cells in the bone marrow often leads to an increase in WBCs in the blood [49]. Blood routine analysis revealed that the leukocyte count in the peripheral blood of the PBS-treated mice was significantly elevated, reaching 8.4-fold greater than that of the healthy mice; however, this increase was completely alleviated after treatment with nanoVi/Vo + nanoCpG (Fig. 3**G**). Importantly, the combination treatment had a limited effect on the levels of red blood cells or platelets (**Fig. S9**).

3.4. *In vivo immunological analysis*

To provide better insight into the role of the nanoVi/Vo + nanoCpG combination in generating *in situ* vaccines and activating the anti-AML immune response, we further analyzed immune cells in the mice on day 21, i.e., one day after the last injection of nanoCpG. The combination treatment significantly increased DC maturation in the lymph nodes, bone marrow and spleen, as evidenced by the elevated expression of costimulatory (CD80/CD86) and antigen presentation molecules (MHC-II) in $CD11c^+$ cells (Fig. 4**A-D and S10**). For example, the percentages of $CD11c^+$ cells with high expression of CD86 or MHC-II in the lymph nodes of mice following combination treatment were increased by 4.3- and 16.5-fold, respectively, relative to those in the PBS group, which was significantly higher than those in the nanoCpG and nanoVi/Vo monotherapy groups (Fig. 4**A, B**). Moreover, markedly increased numbers of mDCs were also observed in the bone marrow, the primary site of AML, of the mice treated with nanoVi/Vo + nanoCpG (Fig. 4**C, D**). Immunofluorescence imaging further demonstrated that the combination treatment group presented the highest proportion of mDCs and the strongest CRT signals in the bone marrow compared with all other groups (Fig. 4**E, F**).

Mature DCs are known to activate T cells, promote T-cell infiltration in the tumor site and modulate the immune response [50,51]. Compared with the other control treatments, the combination treatment significantly increased the numbers of $CD4^+$ T and $CD8^+$ T cells in the spleens of the mice but decreased the number of Tregs (Fig. 4**G-I and S11**). Among the $CD4^+$ T and $CD8^+$ T cells, IFN-γ- and TNF-α-positive T cells were notably increased in the combination group (Fig. 4**J-M**), indicating enhanced activation of T-cell immunity. Moreover, the ratio of $CD8^+$ T cells expressing CD107a (Fig. 4**N**) and perforin (**Fig. S12**), two critical markers of activated cytotoxic T cells, was also significantly greater in the mice treated with nanoVi/Vo + nanoCpG.

The bone marrow microenvironment is an important factor affecting the immunotherapeutic effects of AML. We therefore investigated the ability of nanoVi/Vo + nanoCpG to regulate immune cells in the bone marrow via flow cytometry analysis. Compared with monotherapy, nanoVi/Vo + nanoCpG combination treatment induced a significant increase in the ratio of $CD4^+$ T and $CD8^+$ T cells, resulting in 18.4- and 5.2-fold greater numbers, respectively, than those in PBS-treated mice (Fig. 5**A, B**). Immunofluorescence images provided further evidence that the highest number of $CD8^+$ T cells was observed in the combination treatment group (Fig. 5**C**). More importantly, nanoVi/Vo + nanoCpG outperformed all the other control treatments in increasing the number of $CD8^+$ T cells expressing perforin and granzyme B (Fig. 5**D, E**). In addition, the ratio of M1/M2 macrophages (Fig. 5**F**) in the bone marrow also increased to the highest level after the combination treatment. IFN-γ, TNF-α and IL-12p70 are key proinflammatory cytokines in immunotherapy and can enhance the function of cytotoxic T cells. We next examined their levels in the plasma via ELISA kits. Compared with monotherapy, the combination of nanoVi/Vo and nanoCpG significantly increased the plasma concentrations of IFN-γ, TNF-α and IL-12p70, with 39.7-, 18.4-, and 17.2-fold higher levels, respectively, than those in the PBS group (Fig. 5**G-I**). Collectively, the above results confirmed that nanoVi/Vo can induce ICD in AML cells, which, in combination with nanoCpG, effectively induces an *in situ* vaccination effect and promotes the maturation of DCs and the activation of T cells, eliciting a strong anti-AML immune response.

4. Conclusion

In this work, we demonstrated that an immunogenic vincristine/volasertib dual-drug formulation (nanoVi/Vo) in combination with nanoCpG effectively induced *in situ* vaccination effects and elicited a strong antileukemic immune response *in vivo*. Our strategy conveniently integrates synergistic leukemia inhibition, potent ICD induction and robust immunoadjuvancy, which are advantageous for generating a powerful *in situ* vaccination effect and eliciting strong antitumor immunity. NanoVi/Vo, with a Vi/Vo mass ratio of ca. 1:24, not only synergistically inhibited the proliferation of AML cells with a CI value of ~ 0.3, but also induced strong ICD, boosting the generation of abundant tumor antigens *in situ*. Compared with previously reported ICD-inducing dual-drug nanomedicines that exhibit slow drug release, poor stability or significantly different drug release profiles for two drugs [52,53], disulfide-crosslinked nanoVi/Vo with high stability and rapid intracellular drug corelease is beneficial for synergistic leukemia inhibition and the induction of ICD. The combination of nanoVi/Vo with nanoCpG immunoadjuvant promoted high-efficiency DC maturation and antigen presentation. This combination hence stimulated strong anti-AML immunity in an orthotopic WEHI-3-Luc AML mouse model, as evidenced by the increased recruitment and activation of T cells, reduced Tregs and upregulated levels of proinflammatory cytokines. The combination treatment significantly inhibited leukemia progression in syngeneic AML-bearing mice and markedly improved survival, with 57 % of the

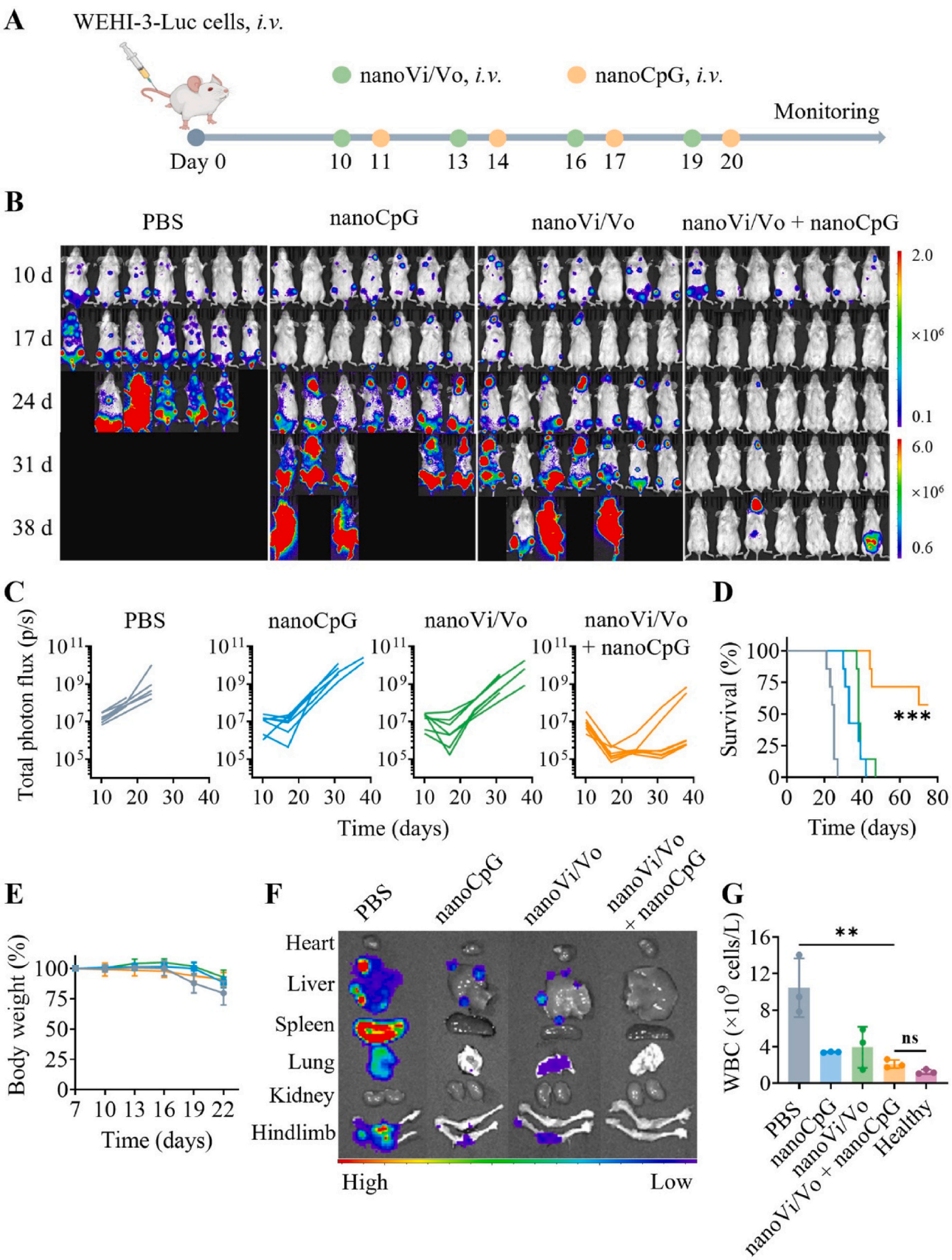

Fig. 3. Immunotherapeutic effect of the combination of nanoVi/Vo and nanoCpG in the orthotopic WEHI-3-Luc model. PBS, nanoVi/Vo or nanoCpG served as controls. (A) Schematic of the treatment schedules. (B) Bioluminescence images and (C) quantitative analysis of the mice following different treatments. (D) Survival curves (***$p < 0.001$) and (E) body weight changes of the mice following different treatments ($n = 7$). (F) Ex vivo bioluminescence imaging of major organs and hindlimbs from different groups. (G) Proportion of white blood cells (WBCs) in the blood of the mice in the different groups ($n = 3$, **$p < 0.01$).

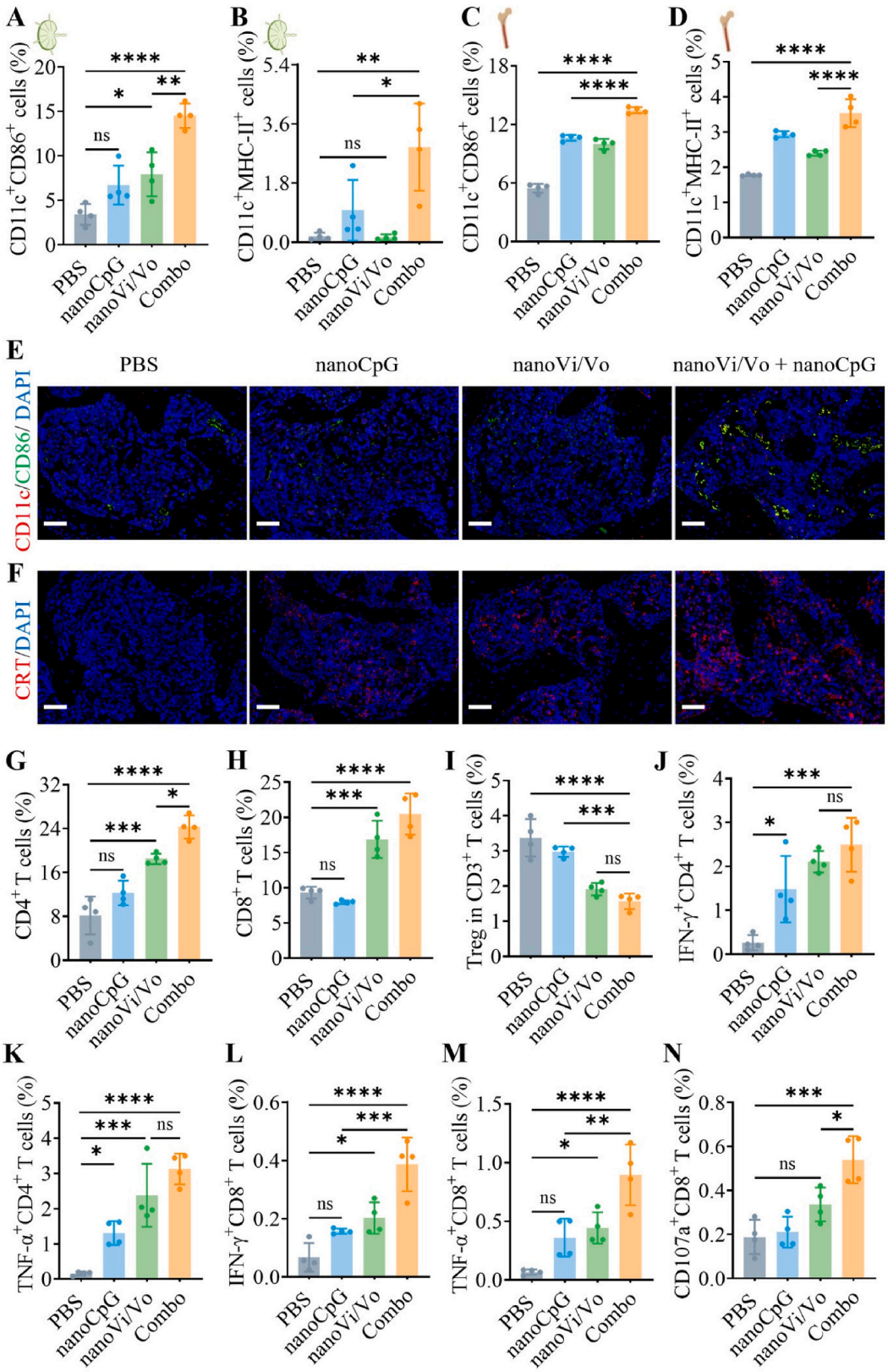

Fig. 4. DC activation and splenic immune cell analysis. Proportions of (A) $CD11c^+CD86^+$ DCs and (B) $CD11c^+MHC\text{-}II^+$ DCs in the lymph nodes (n = 4). Percentages of (C) $CD11c^+CD86^+$ DCs and (D) $CD11c^+MHC\text{-}II^+$ DCs in the bone marrow (n = 4). Representative immunofluorescence images showing (E) the distribution of $CD11c^+CD86^+$ DCs and (F) CRT expression in the hindlimb slices. Percentages of (G) $CD3^+CD4^+$ T cells, (H) $CD3^+CD8^+$ T cells and (I) $CD3^+CD4^+FoxP3^+$ Tregs in the spleen across different treatment groups (n = 4). The proportions of (J, K) $CD4^+$ T cells and (L, M) $CD8^+$ T cells that secreted IFN-γ and TNF-α in the spleen (n = 4). (N) Proportion of CD107a-positive CTL cells in the spleen (n = 4). Scale bars: 50 μm. Combo denotes nanoVi/Vo + nanoCpG. *$p < 0.05$, **$p < 0.01$, ***$p < 0.001$, ****$p < 0.0001$.

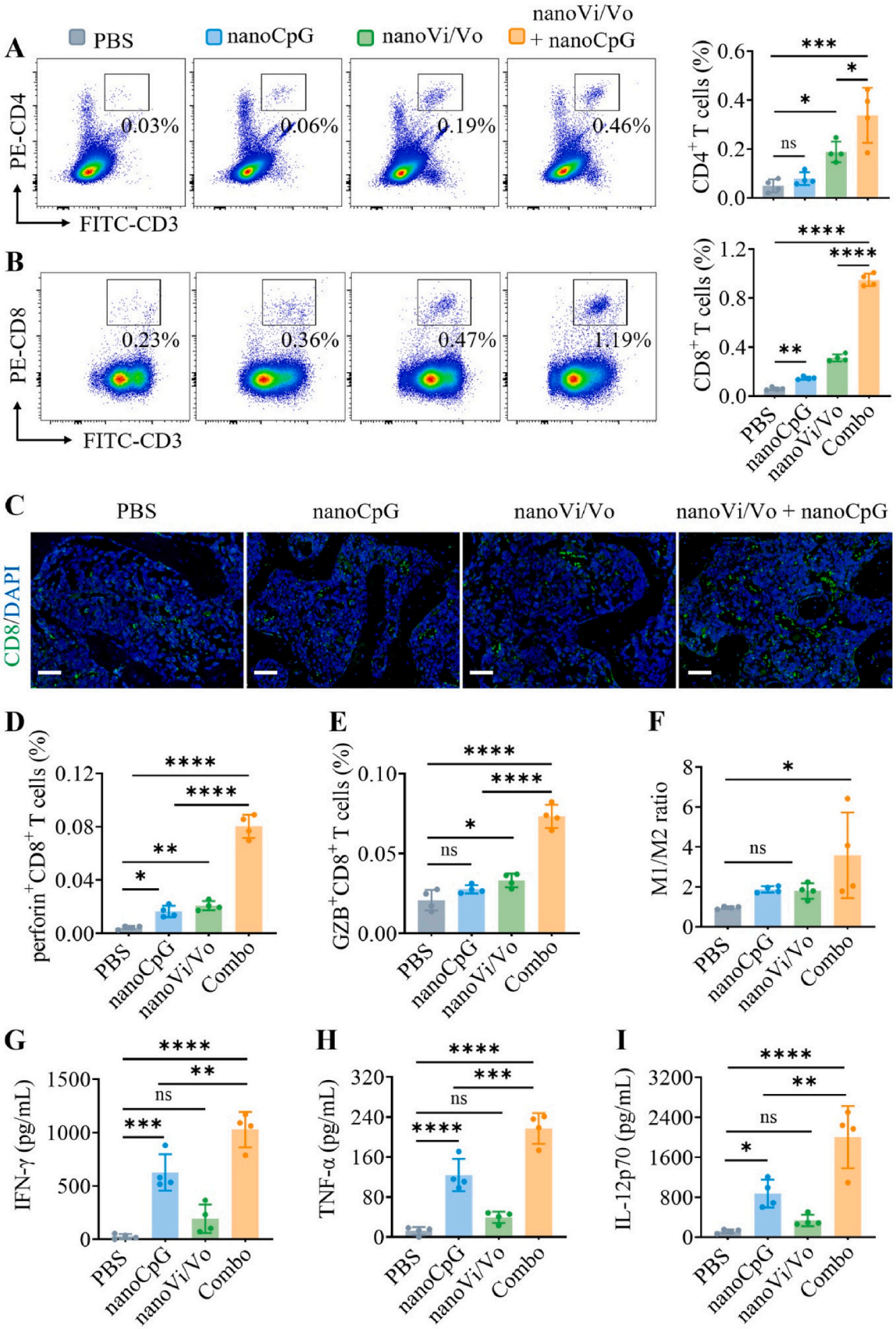

Fig. 5. Representative flow cytometry plots and quantitative analyses of (A) $CD4^+$ T cells and (B) $CD8^+$ T cells in the bone marrow (n = 4). (C) Representative immunofluorescence images of $CD8^+$ T cells in leg bone sections. Scale bar, 50 μm. The proportions of CTLs that secreted (D) perforin and (E) granzyme B (GZB) in the bone marrow, as well as the ratios of (F) M1/M2 macrophages (n = 4). The concentrations of (G) IFN-γ, (H) TNF-α, and (I) IL-12p70 in the serum of mice from different treatment groups (n = 4). Combo denotes nanoVi/Vo + nanoCpG. *p < 0.05, **p < 0.01, ***p < 0.001, ****p < 0.0001.

mice achieving long-term survival, outperforming all the control groups. Compared with personalized anti-leukemia vaccines, which are associated with individual tailoring, tedious processing and inconsistent quality [13,54], this work innovatively combines synergistic ICD nanoinducers and CpG nanoadjuvants to overcome these challenges and generate vaccines *in situ*. Given the broad-spectrum antitumor activity of vincristine and the overexpression of PLK1 in diverse types of malignancies, future work will further investigate the therapeutic effects and applicability of this combinatorial strategy in treating other blood cancers and solid tumors. Overall, this study provides a powerful *in situ* vaccination strategy that may potentiate immunotherapy for AML and other malignancies.

CRediT authorship contribution statement

Lanlan Liang: Writing – original draft, Methodology, Investigation, Formal analysis, Data curation. **Zhenzhen Zhai:** Methodology, Investigation, Formal analysis. **Wenhai Lin:** Writing – review & editing, Methodology. **Li Cao:** Methodology. **Huanli Sun:** Writing – review & editing, Supervision, Project administration, Funding acquisition, Conceptualization. **Zhiyuan Zhong:** Writing – review & editing, Supervision, Project administration, Funding acquisition, Conceptualization.

Declaration of competing interest

The authors declare that they have no known competing financial interests or personal relationships that could have appeared to influence the work reported in this paper.

Acknowledgment

This work was supported by the National Natural Science Foundation of China (52273251, 52473264 and 52233007). The schemes in the figures were created with BioRender.com.

Appendix A. Supplementary data

Supplementary data to this article can be found online at https://doi.org/10.1016/j.jcis.2025.138144.

Data availability

Data will be made available on request.

References

[1] C.D. DiNardo, H.P. Erba, S.D. Freeman, A.H. Wei, Acute myeloid leukaemia, Lancet 401 (2023) 2073–2086.
[2] H.M. Kantarjian, C.D. DiNardo, T.M. Kadia, N.G. Daver, J.K. Altman, E.M. Stein, E. Jabbour, C.A. Schiffer, A. Lang, F. Ravandi, Acute myeloid leukemia management and research in 2025, CA Cancer J. Clin. 75 (2025) (2025) 46–67.
[3] J. Schaefer, S. Cassidy, R.M. Webster, The acute myeloid leukaemia market, Nat. Rev. Drug Discov. 19 (2020) 233–234.
[4] H. Döhner, A.H. Wei, B. Löwenberg, Towards precision medicine for AML, Nat. Rev. Clin. Oncol. 18 (2021) 577–590.
[5] X. Xie, Y. Hu, T. Ye, Y. Chen, L. Zhou, F. Li, X. Xi, S. Wang, Y. He, X. Gao, W. Wei, G. Ma, Y. Li, Therapeutic vaccination against leukaemia via the sustained release of co-encapsulated anti-PD-1 and a leukaemia-associated antigen, Nat. Biomed. Eng. 5 (2021) 414–428.
[6] R.S. Bhansali, K.W. Pratz, C. Lai, Recent advances in targeted therapies in acute myeloid leukemia, J. Hematol. Oncol. 16 (2023) 29.
[7] A.S. Bhagwat, L. Torres, O. Shestova, M. Shestov, P.W. Mellors, H.R. Fisher, S. N. Farooki, B.F. Frost, M.R. Loken, A.L. Gaymon, D. Frazee, W. Rogal, N. Frey, E. O. Hexner, S.M. Luger, A.W. Loren, M.E. Martin, S.R. McCurdy, A.E. Perl, E. A. Stadtmauer, J.L. Brogdon, J.A. Fraietta, W.-T. Hwang, D.L. Siegel, G. Plesa, R. Aplenc, D.L. Porter, C.H. June, S.I. Gill, Cytokine-mediated CAR t therapy resistance in AML, Nat. Med. 30 (2024) 3697–3708.
[8] J. Liu, M. Fu, M. Wang, D. Wan, Y. Wei, X. Wei, Cancer vaccines as promising immuno-therapeutics: Platforms and current progress, J. Hematol. Oncol. 15 (2022) 28.
[9] M. Saxena, S.H. van der Burg, C.J.M. Melief, N. Bhardwaj, Therapeutic cancer vaccines, Nat. Rev. Cancer 21 (2021) 360–378.
[10] M.C. Sellars, C.J. Wu, E.F. Fritsch, Cancer vaccines: Building a bridge over troubled waters, Cell 185 (2022) 2770–2788.
[11] N. Wang, G. Zhang, H. Sun, Y. Tian, J. Hao, J. Cui, Vaccine nanoparticles derived from mung beans for cancer immunotherapy, Chem. Mater. 33 (2021) 4057–4066.
[12] D.-S. Kuen, J. Hong, S. Lee, C.-H. Koh, M. Kwak, B.-S. Kim, M. Jung, Y.-J. Kim, B.-S. Cho, B.-S. Kim, Y. Chung, A personalized cancer vaccine that induces synergistic innate and adaptive immune responses, Adv. Mater. 35 (2023) 2303080.
[13] P. Zhang, T. Wang, G. Cui, R. Ye, W. Wan, T. Liu, Y. Zheng, Z. Zhong, Systemic multifunctional nanovaccines for potent personalized immunotherapy of acute myeloid leukemia, Adv. Mater. 36 (2024) 2407189.
[14] P.D. Katsikis, K.J. Ishii, C. Schliehe, Challenges in developing personalized neoantigen cancer vaccines, Nat. Rev. Immunol. 24 (2024) 213–227.
[15] T. Fan, M. Zhang, J. Yang, Z. Zhu, W. Cao, C. Dong, Therapeutic cancer vaccines: Advancements, challenges and prospects, Sig. Transduct. Target. Ther. 8 (2023) 450.
[16] N. Gong, M.-G. Alameh, R. El-Mayta, L. Xue, D. Weissman, M.J. Mitchell, Enhancing in situ cancer vaccines using delivery technologies, Nat. Rev. Drug Discov. 23 (2024) 607–625.
[17] G. Niu, H. Wang, Y. Zhai, B. Zhou, Y. Kang, Z. Pei, X. Ji, Nanotechnology-based in situ cancer vaccines: Mechanisms, design, and recent advances, Nano Today 56 (2024) 102286.
[18] L. Galluzzi, A. Buqué, O. Kepp, L. Zitvogel, G. Kroemer, Immunogenic cell death in cancer and infectious disease, Nat. Rev. Immunol 17 (2017) 97–111.
[19] Z. Li, X. Lai, S. Fu, L. Ren, H. Cai, H. Zhang, Z. Gu, X. Ma, K. Luo, Immunogenic cell death activates the tumor immune microenvironment to boost the immunotherapy efficiency, Adv. Sci. 9 (2022) 2201734.
[20] H. Pan, P. Liu, L. Zhao, Y. Pan, M. Mao, G. Kroemer, O. Kepp, Immunogenic cell stress and death in the treatment of cancer, Semin. Cell Dev. Biol. 156 (2024) 11–21.
[21] H. Wang, A.J. Najibi, M.C. Sobral, B.R. Seo, J.Y. Lee, D. Wu, A.W. Li, C.S. Verbeke, D.J. Mooney, Biomaterial-based scaffold for in situ chemo-immunotherapy to treat poorly immunogenic tumors, Nat. Commun. 11 (2020) 5696.
[22] G. Kroemer, C. Galassi, L. Zitvogel, L. Galluzzi, Immunogenic cell stress and death, Nat. Immunol. 23 (2022) 487–500.
[23] L. Galluzzi, O. Kepp, E. Hett, G. Kroemer, F.M. Marincola, Immunogenic cell death in cancer: Concept and therapeutic implications, J. Transl. Med. 21 (2023) 162.
[24] S. Zhang, H. Zhou, Y. Liu, G. Chen, Q. Li, Y. Xu, R. Zheng, S. Li, X. Chen, L. Zhao, A stimuli–responsive immunostimulant to activate chemo-immunotherapeutic effects by inducing DNA damage and sting activation, J. Colloid Interface Sci. 688 (2025) 664–676.
[25] G.M. Dogheim, N.E. El Feel, E.A. Abd El-Maksod, S.S. Amer, S.A. El-Gizawy, A. S. Abd Elhamid, A.O. Elzoghby, Nanomedicines as enhancers of tumor immunogenicity to augment cancer immunotherapy, Drug Discovery Today 29 (2024) 103905.
[26] A.O. Elzoghby, O. Samir, H.E. Emam, A. Soliman, R.M. Abdelgalil, Y. M. Elmorshedy, K.A. Elkhodairy, M.L. Nasr, Engineering nanomedicines for immunogenic eradication of cancer cells: Recent trends and synergistic approaches, Acta Pharm. Sin. B 14 (2024) 2475–2504.
[27] R. Demuynck, Y. Engelen, A.G. Skirtach, S.C. De Smedt, I. Lentacker, D.V. Krysko, Nanomedicine to aid immunogenic cell death (ICD)-based anticancer therapy, Trends, Cancer 10 (2024) 486–489.
[28] J. Jeon, B. Yoon, A. Dey, S.H. Song, Y. Li, H. Joo, J.H. Park, Self-immolative polymer-based immunogenic cell death inducer for regulation of redox homeostasis, Biomaterials 295 (2023) 122064.
[29] R.E.A. Gutteridge, M.A. Ndiaye, X. Liu, N. Ahmad, Plk1 inhibitors in cancer therapy: From laboratory to clinics, Mol. Cancer Ther. 15 (2016) 1427–1435.
[30] J. Zhang, L. Zhang, J. Wang, L. Ouyang, Y. Wang, Polo-like kinase 1 inhibitors in human cancer therapy: Development and therapeutic potential, J. Med. Chem. 65 (2022) 10133–10160.
[31] X. Zhang, B. Yang, Q. Ni, X. Chen, Materials engineering strategies for cancer vaccine adjuvant development, Chem. Soc. Rev. 52 (2023) 2886–2910.
[32] B. Pulendran, P.S. Arunachalam, D.T. O'Hagan, Emerging concepts in the science of vaccine adjuvants, Nat. Rev. Drug Discov. 20 (2021) 454–475.
[33] J. Vollmer, A.M. Krieg, Immunotherapeutic applications of CpG oligodeoxynucleotide TLR9 agonists, Adv. Drug Deliv. Rev. 61 (2009) 195–204.
[34] B. Guo, Y. Qu, Y. Sun, S. Zhao, J. Yuan, P. Zhang, Z. Zhong, F. Meng, Co-delivery of gemcitabine and paclitaxel plus NanoCpG empowers chemoimmunotherapy of postoperative "cold" triple-negative breast cancer, Bioact. Mater. 25 (2023) 61–72.
[35] N. Yu, Y. Zhang, J. Li, W. Gu, S. Yue, B. Li, F. Meng, H. Sun, R. Haag, J. Yuan, Z. Zhong, Daratumumab immunopolymersome-enabled safe and CD38-targeted chemotherapy and depletion of multiple myeloma, Adv. Mater. 33 (2021) 2007787.
[36] P. Yao, Y. Zhang, H. Meng, H. Sun, Z. Zhong, Smart polymersomes dually functionalized with cRGD and fusogenic GALA peptides enable specific and high-efficiency cytosolic delivery of apoptotic proteins, Biomacromolecules 20 (2019) 184–191.
[37] Q. Deng, S. Yue, F. You, Z. Zhai, H. Sun, L. Liang, C. Li, L. Yang, Z. Zhong, Vincristine/volasertib polymersome injection enables high-efficiency synergistic treatment of acute lymphoblastic leukemia, Acta Biomater. (2025), https://doi.org/10.1016/j.actbio.2025.1005.1041.
[38] C.M. Jogdeo, S. Panja, S. Kanvinde, E. Kapoor, K. Siddhanta, D. Oupický, Advances in lipid-based codelivery systems for cancer and inflammatory diseases, Adv. Healthcare Mater. 12 (2023) 2202400.

[39] A. Detappe, H.V.T. Nguyen, Y. Jiang, M.P. Agius, W. Wang, C. Mathieu, N.K. Su, S. L. Kristufek, D.J. Lundberg, S. Bhagchandani, I.M. Ghobrial, P.P. Ghoroghchian, J. A. Johnson, Molecular bottlebrush prodrugs as mono- and triplex combination therapies for multiple myeloma, Nat. Nanotechnol. 18 (2023) 184–192.
[40] J. Du, S. Yue, C. Li, J. Li, S. Zhao, Y. Dong, Y. Zhang, R. Cheng, H. Sun, Z. Zhong, Exogenous CD38 upregulation enables high-efficacy dually cascade targeted molecular therapy of leukemia, Nano Today 50 (2023) 101872.
[41] S. Yue, J. An, Y. Zhang, J. Li, C. Zhao, J. Liu, L. Liang, H. Sun, Y. Xu, Z. Zhong, Exogenous antigen upregulation empowers antibody targeted nanochemotherapy of leukemia, Adv. Mater. 35 (2023) 2209984.
[42] C. Zhou, Y. Xia, Y. Wei, L. Cheng, J. Wei, B. Guo, F. Meng, S. Cao, J.C.M. van Hest, Z. Zhong, GE11 peptide-installed chimaeric polymersomes tailor-made for high-efficiency EGFR-targeted protein therapy of orthotopic hepatocellular carcinoma, Acta Biomaterialia 113 (2020) 512–521.
[43] S. Shelake, U.T. Sankpal, D. Eslin, W.P. Bowman, J.W. Simecka, S. Raut, A. Ray, R. Basha, Clotam enhances anti-proliferative effect of vincristine in ewing sarcoma cells, Apoptosis 24 (2019) 21–32.
[44] J. Van den Bossche, F. Lardon, V. Deschoolmeester, I. De Pauw, J.B. Vermorken, P. Specenier, P. Pauwels, M. Peeters, A. Wouters, Spotlight on volasertib: Preclinical and clinical evaluation of a promising plk1 inhibitor, Med. Res. Rev. 36 (2016) 749–786.
[45] J. Zhou, Q. Yang, L. Lu, Z. Tuo, Z. Shou, J. Cheng, PLK1 inhibition induces immunogenic cell death and enhances immunity against NSCLC, Int. J. Med. Sci. 18 (2021) 3516–3525.
[46] J. Wei, D. Wu, S. Zhao, Y. Shao, Y. Xia, D. Ni, X. Qiu, J. Zhang, J. Chen, F. Meng, Z. Zhong, Immunotherapy of malignant glioma by noninvasive administration of TLR9 agonist CpG nano-immunoadjuvant, Adv. Sci. 9 (2022) 2103689.
[47] Q. Li, R. Su, X. Bao, K. Cao, Y. Du, N. Wang, J. Wang, F. Xing, F. Yan, K. Huang, S. Feng, Glycyrrhetinic acid nanoparticles combined with ferrotherapy for improved cancer immunotherapy, Acta Biomater. 144 (2022) 109–120.
[48] H. Bai, T. Wang, F. Kong, M. Zhang, Z. Li, L. Zhuang, M. Ma, F. Liu, C. Wang, H. Xu, N. Gu, Y. Zhang, CXCR4 and CD44 dual-targeted prussian blue nanosystem with daunorubicin loaded for acute myeloid leukemia therapy, Chem. Eng. J. 405 (2021) 126891.
[49] X. Wang, R. Huang, W. Wu, J. Xiong, Q. Wen, Y. Zeng, T. Chen, J. Li, C. Zhang, J. F. Zhong, S. Yang, X. Zhang, Amplifying sting activation by bioinspired nanomedicine for targeted chemo- and immunotherapy of acute myeloid leukemia, Acta Biomater. 157 (2023) 381–394.
[50] B.W. MacNabb, X. Chen, S. Tumuluru, J. Godfrey, D.N. Kasal, J. Yu, M.L. M. Jongsma, R.M. Spaapen, D.E. Kline, J. Kline, Dendritic cells can prime anti-tumor CD8+ T cell responses through major histocompatibility complex cross-dressing, Immunity 55 (2022) 982–997.
[51] M.J. Pittet, M. Di Pilato, C. Garris, T.R. Mempel, Dendritic cells as shepherds of T cell immunity in cancer, Immunity 56 (2023) 2218–2230.
[52] M. Chen, Y. Qiao, J. Cao, L. Ta, T. Ci, X. Ke, Biomimetic doxorubicin/ginsenoside co-loading nanosystem for chemoimmunotherapy of acute myeloid leukemia, J. Nanobiotechnol. 20 (2022) 273.
[53] V. Krishnan, V. Dharamdasani, S. Bakre, V. Dhole, D. Wu, B. Budnik, S. Mitragotri, Hyaluronic acid nanoparticles for immunogenic chemotherapy of leukemia and t-cell lymphoma, Pharmaceutics 14 (2022) 466.
[54] M.R. Nahas, D. Stroopinsky, J. Rosenblatt, L. Cole, A.R. Pyzer, E. Anastasiadou, A. Sergeeva, A. Ephraim, A. Washington, S. Orr, M. McMasters, M. Weinstock, S. Jain, R.K. Leaf, H. Ghiasuddin, M. Rahimian, J. Liegel, J.J. Molldrem, F. Slack, D. Kufe, D. Avigan, Hypomethylating agent alters the immune microenvironment in acute myeloid leukaemia (AML) and enhances the immunogenicity of a dendritic cell/AML vaccine, Br. J. Haematol. 185 (2019) 679–690.